THE JOURNAL OF PHYSICAL CHEMISTRY A

Feature Article

pubs.acs.org/JPCA

Cluster Model Studies of Anion and Molecular Specificities via Electrospray Ionization Photoelectron Spectroscopy

Xue-Bin Wang*,†

†Physical Sciences Division, Pacific Northwest National Laboratory, P.O. Box 999, MS K8-88, Richland, Washington 99352, United States

ABSTRACT: Ion specificity, a widely observed macroscopic phenomenon in condensed phases and at interfaces, is a fundamental chemical physics issue. Herein we report our recent studies of such effects using cluster models in an "atom-by-atom" and "molecule-by-molecule" fashion not possible with the condensed-phase methods. We use electrospray ionization (ESI) to generate molecular and ionic clusters to simulate key molecular entities involved in local binding regions and characterize them by employing negative ion photoelectron spectroscopy (NIPES). Inter- and intramolecular interactions and binding configurations are directly obtained as functions of the cluster size and composition, providing molecular-level descriptions and characterization over the local active sites that play crucial roles in determining the solution chemistry and condensed-phase phenomena. The topics covered in this article are relevant to a wide range of research fields from ion specific effects in electrolyte solutions, ion selectivity/recognition in normal functioning of life, to molecular specificity in aerosol particle formation, as well as in rational material design and synthesis.

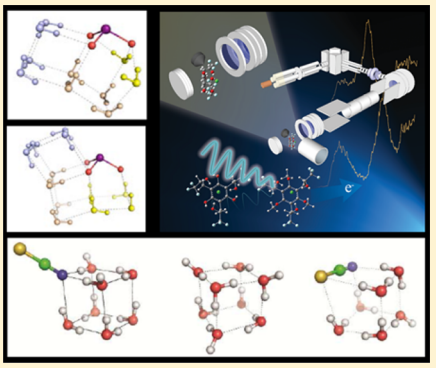

1. INTRODUCTION

Many important chemical reactions and transformations, including biologically relevant processes, atmospheric aerosol chemistry, homogeneous catalytic reactions, and environmental/geological processes, take place in solutions and at interfaces. Fundamental understanding of solution chemistry and condensed-phase phenomena is of great scientific and practical interest.[1−3] However, the complications of the bulk environment present considerable challenges for obtaining a molecular or local description of phenomena in the solution phase. Gas-phase cluster studies with precisely defined numbers of solvent molecules and molecular specificity are ideal in providing microscopic information on macroscopic phenomena, which are highly amenable to modeling with high level theoretical methods. The absence of the bulk environment and media often amplifies effects of solute−solvent interactions and local binding configuration within active sites, exposing insights that may not be possible to resolve with bulk observations.

Several gas-phase techniques combined with theoretical calculations have been developed to investigate solvated species.[4−23] A major advance in the study of solution-phase species, in particular, multiply charged anions (MCAs), was achieved by the coupling of electrospray ionization (ESI) with negative ion photoelectron spectroscopy (NIPES), in which ESI is employed to generate MCAs, pristine solution-phase species, and solvated clusters directly from solution samples; NIPES is used to directly probe their electronic structures, stability, and energetics.[24,25] Significant progresses have been achieved in this direction to examine the electronic structures and stabilities for a wide variety of solution-phase anion species ranging from inorganic oxoanions and metal complexes to conjugated bases of organic acids and biological molecules and have been previously reviewed in several publications.[26−30] This article instead focuses on our recent ESI-NIPES research activities at PNNL using size-selected and composition-tailored binary and ternary clusters as model systems to probe fundamental molecular interactions among complex anions, solvents, substrate molecules, and counterions at play that largely determine condensed phases chemistry and phenomena.[31−42] Specifically, we have drawn our attention on obtaining molecular-level understanding of noncovalent intermolecular interactions that are responsible for a wide range of macroscopically observed phenomena. Such phenomena include ion specific effects where different solute molecules exhibit markedly different solvation characteristics and binding ability; specific binding in host−guest chemistry where guest anions and host substrate molecules display pronounced molecular fidelity and recognition, and molecular specificity in the early stages of aerosol particle formation where the involvement of certain types of molecules significantly facilitates and promotes initial nucleation processes.

2. EXPERIMENTAL METHODS AND INTERMOLECULAR INTERACTION ANALYSES

The ESI-NIPES apparatus developed at PNNL couples an ESI source and a cryogenic ion-trap time-of-flight (TOF) mass spectrometry with a magnetic-bottle TOF photoelectron spectrometer.[24] We employ ESI to generate solution-phase species including MCAs and solvated clusters with desired compositions and size distributions directly from solution samples and

Received: September 27, 2016
Revised: December 1, 2016
Published: January 6, 2017

DOI: 10.1021/acs.jpca.6b09784
J. Phys. Chem. A 2017, 121, 1389−1401

transport them into the gas phase. NIPES is used to probe their electronic structures, stability, energetics, as well as the variation of these properties as functions of size and composition with atomic-level precision. The advancement in cooling and controlling cluster temperature using the generic cryogenic ion trap has eliminated vibrational hot bands, improved spectral resolution,[43−46] and made it possible to study different isomer populations and conformational changes as a function of temperature.[47−51]

Figure 1 gives a schematic overview of this apparatus. The desired anions and anionic clusters are generated by spraying

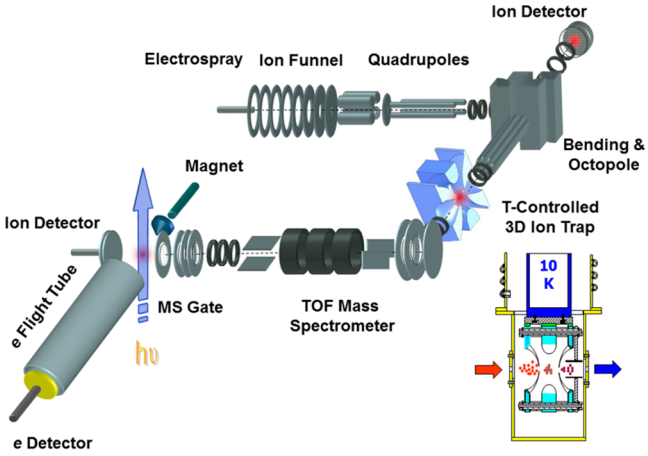

Figure 1. Schematic drawing of the PNNL ESI-NIPES apparatus with the cryogenic ion trap shown in the inset.

$\sim 10^{-3}$ M aqueous methanol/acetonitrile solutions containing the anions of interest. All the anions and anionic clusters produced by ESI at ambient conditions are then transported and guided by two radio frequency quadruple ion guides followed by a 90° bender into a 3-D temperature-controlled ion trap (Figure 1 inset), where they are accumulated and cooled via collisions with a cold buffer gas (20% H_2 balanced in He) before being pulsed out into the extraction zone of a TOF mass spectrometer at a 10 Hz repetition rate. For each NIPES experiment, the ESI source conditions are first optimized to maximize the mass intensity of the desired anions and clusters monitored by the quadruple mass spectrometry and the TOF mass spectrometer, and then the anions of interest are mass selected and decelerated before being photodetached with a laser beam using 355/266 nm photons from Nd:YAG, or 193/157 nm photons from an excimer laser in the detachment zone of the magnetic bottle photoelectron analyzer. The laser is operated at a 20 Hz repetition rate with the ion beam off at alternating laser shots, affording shot-by-shot background subtraction. Photoelectrons are collected at nearly 100% efficiency by the magnetic bottle and analyzed by a 5.2 m long electron flight tube. The time-of-flight photoelectron spectra are collected and converted to kinetic energy spectra calibrated with the known spectra of I^- and $Cu(CN)_2^-$. The electron binding energy (EBE) spectra are obtained by subtracting the kinetic energy spectra from the detachment photon energies. The best energy resolution obtained for I^- after full ion deceleration is ca. 20 meV full width at half-maximum (fwhm) for 1 eV electrons. The adiabatic detachment energy (ADE) is obtained from the 0−0 transition for vibrationally resolved spectra, or by adding the instrumental resolution to the EBE at the crossing point of the onset of the spectral feature and the baseline for the spectra without resolved vibrational structures. On the contrary, the vertical detachment energy (VDE) is measured from the spectral maximum of the first band assigned to the transition from the ground state of the anion to the ground state of the neutral. The experimental ADE and VDE can be directly compared to the theoretical ADE and VDE, which are calculated as the energy differences between the neutral and anion at their respective optimized neutral and anion's geometries for the former, and with the neutral and anion both at the fixed anion's geometry for the latter.

Considering an anion solute A^- solvated by solvent molecule(s) S, the key experimental data obtained from NIPES studies of A^- and $[A^-\cdot S]$ is the EBE difference between $[A^-\cdot S]$ and A^-, i.e., $EBE(A^-\cdot S) - EBE(A^-)$, which is equal to the binding energy (BE) difference between A^- with S and $A^\bullet$ (the photodetached A^-) with S (Figure 2). It is often the case that the

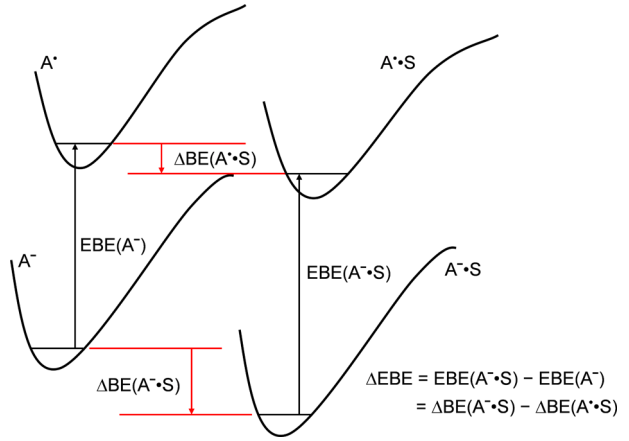

Figure 2. Schematic interpretation of the relationship between the electron binding energy (EBE) difference and the binding energy (BE) difference of solute anion A^- and neutral $A^\bullet$ with solvent molecule(s) S.

interaction of the anion and the solvent is stronger than that of the neutral and the solvent, i.e., $BE(A^-\cdot S) > BE(A^\bullet\cdot S)$, leading to a stepwise increase in EBE upon clustering with each solvent molecule. The EBE increase can be approximated as the interaction energy between the solute anion and solvent/substrate molecule if the corresponding BE of the neutral and solvent/substrate molecule is significantly smaller. However, it is more interesting that in some cases, as shown in section 3 below, there is nearly no increase or even decrease in EBE when one additional solvent molecule is subsequently added on, suggesting that $BE(A^\bullet\cdot S)$ is equal to or larger than $BE(A^-\cdot S)$. Observation of such an "abnormality" is indicative of a special binding motif that favors the $A^\bullet$ and S interaction. Therefore, NIPES is a powerful experimental technique that can directly yield energetic binding information not only between the solute anion and solvent/substrate but also for the neutral and solvent, which are sensitive to local binding configurations of guest anion (A^-) and neutral ($A^\bullet$) with host molecules (S).

3. ANION SPECIFICITY IN HYDRATED CLUSTERS: CLUSTER MODEL INSIGHTS ON HOW KOSMOTROPE AND CHAOTROPE ANIONS GUIDE THE LOCAL SOLVATION STRUCTURE OF WATER

Many phenomena occurring in condensed phases (like colloids, polymers, interfaces, and biological systems) that involve

DOI: 10.1021/acs.jpca.6b09784
J. Phys. Chem. A 2017, 121, 1389−1401

electrolytes show pronounced ion specificity—phenomena where different solute molecules exhibit markedly different solvation characteristics. A well-known example of such behavior can be found in the much discussed Hofmeister series (Figure 3),

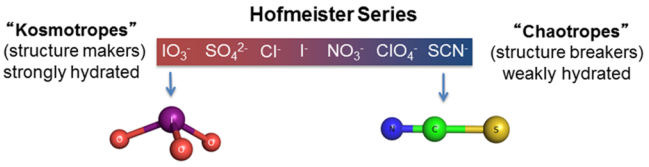

Figure 3. Short list of the anion Hofmeister series.

in which the behavior of charged solute molecules in aqueous solutions is often classified using the concept of kosmotropes ("structure makers") and chaotropes ("structure breakers") to describe strongly and weakly hydrated anions, respectively.[52−57] There is a growing consensus that the key to kosmotropic/chaotropic behavior lies in the local solvent region,[53,55] but the exact microscopic basis for such differentiation is not well understood.

We have examined this issue by carrying out cluster model studies on IO_3^- and SCN^- anion solvation.[31,32] We chose these two anions because they both are singly charged and possess similar molecular sizes and polarizabilities,[56] but the former, IO_3^-, is classified as a kosmotrope anion (strongly hydrated)[58] and the latter, SCN^-, is a typical chaotrope (weakly hydrated)[56] (Figure 3). We wanted to know how the local solvent structure of water changes by the insertion of these two representative anions. Such information is expected to provide much needed insight into bridge the macroscopically observed Hofmeister series with molecular level description.

3.1. $IO_3^-(H_2O)_n$ (n = 0−12) Clusters: A Kosmotrope Case. Figure 4 shows the experimental photoelectron spectra of $IO_3^-(H_2O)_{n=0-12}$ clusters (left), as well as the experimental and computed values of the EBE and their incremental differences, $\Delta EBE(n) = EBE(n) - EBE(n-1)$, as a function of cluster size n (right).[31] The spectra of the solvated clusters exhibit spectral patterns similar to that of IO_3^- but show a stepwise increase in EBE with the number of water molecules up to n = 9. However, at n = 10, the EBE displays an unexpected drop and then continues to increase for n = 11−12 clusters. Ab initio calculations reproduce the observed experimental trends in the EBE, also indicating a drop at n = 10 (Figure 4 right). Minimum energy structures show that the evolution of IO_3^- solvation proceeds in a cyclical fashion by building water tetramer layers, initially starting at the negatively charged oxygen side, and eventually coming into contact with the cationic iodine side (Figure 5). The gradual buildup of the solvent network from a bidentate to the water tetramer structure observed in n = 1−4 clusters (blue) recurs for n = 5−8 (brown) and 9−12 (yellow), and in such a way that the original tetramer solvent layer rotates out of way to accommodate the growth of the new ones. As a *kosmotrope* anion, IO_3^- can organize solvent water molecules via a cyclic water network around it and hence is a "*structure maker*".

The decrease of EBE during the solvation of rigid anion solutes is unprecedented. To understand the origin of this seemingly anomalous event, we define the cluster growth energy:

$$\Delta E(n) = E(n) - E(n-1) - E^{w} \quad (1)$$

a difference between total energy of n and $n-1$ clusters, referenced to the energy of the single water molecule (E^w) (i.e., the nth water binding energy), allowing the ΔEBE to be rewritten in the following form:

$$\Delta EBE(n) = \Delta E^{neutr}(n) - \Delta E^{anion}(n) \quad (2)$$

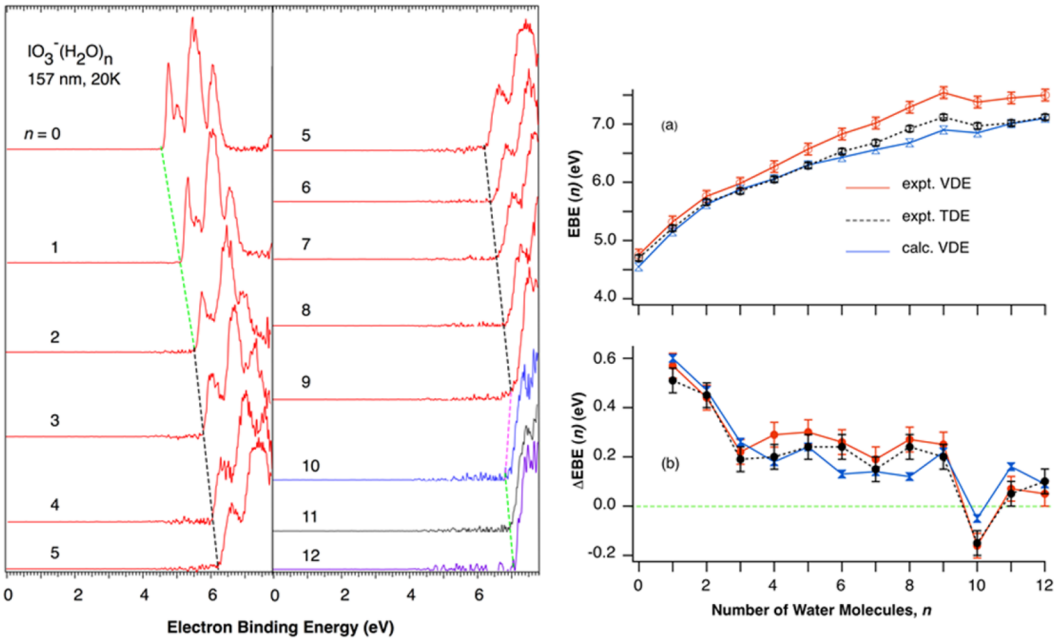

Figure 4. (Left) photoelectron spectra of $IO_3^-(H_2O)_n$ (n = 0−12) at 157 nm (7.867 eV) and 20 K. Note the monotonic increase of electron binding energy (EBE) from n = 0 to 9, and a decrease at n = 10, followed by a marginal increase again for n = 11 and 12 as guided in colored dashed lines along each spectral threshold (which defines the threshold detachment energy, TDE). (Right) (a) EBE (n) and (b) incremental differences, $\Delta EBE(n) = EBE(n) - EBE(n-1)$, as a function of the number of water molecules, n. TDE(n) and ΔTDE(n) are also plotted for comparison. The calculated VDE(n) and ΔVDE(n) from the minimum structures (Figure 5) are presented and compared to the experimental values. Reproduced from ref 31 with permission from AIP Publishing LLC. Copyright 2013.

DOI: 10.1021/acs.jpca.6b09784
J. Phys. Chem. A 2017, 121, 1389−1401

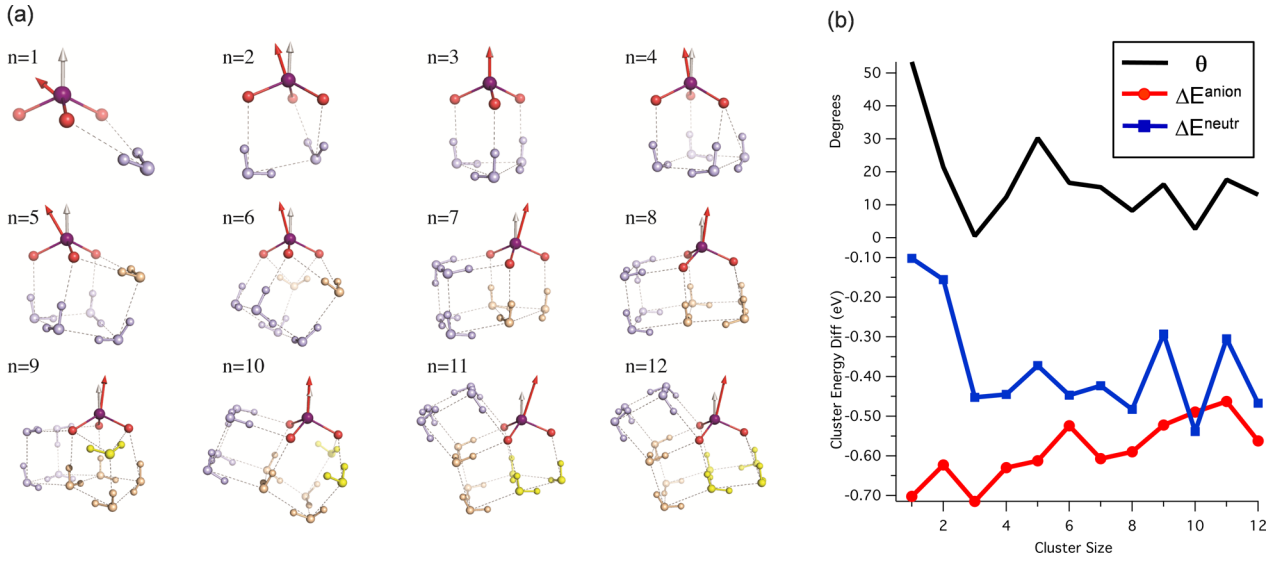

Figure 5. (a) Minimum energy structures for $IO_3^-(H_2O)_n$ (n = 0−12) clusters obtained from ab initio calculations. The initial solvation evolves from bidentate water to the water tetramer network in n = 1−4 (blue). This solvation scheme recurs for n = 5−8 (brown) and 9−12 (yellow) with the previously formed tetramer layers simultaneously rotated out of the way to accommodate the addition of new water molecules. The dipole vectors of the solute (silver arrow) and solvent network (red arrow) for each structure are indicated. (b) (top) angle between solvent electric field and iodate axis of symmetry at the center of mass (black). (Bottom) ab initio energy differences for anion (red) and neutral (blue) iodate water clusters as a function of cluster size. The reference energy of water was set at −76.43413 au. Reproduced from ref 31 with permission from AIP Publishing LLC. Copyright 2013.

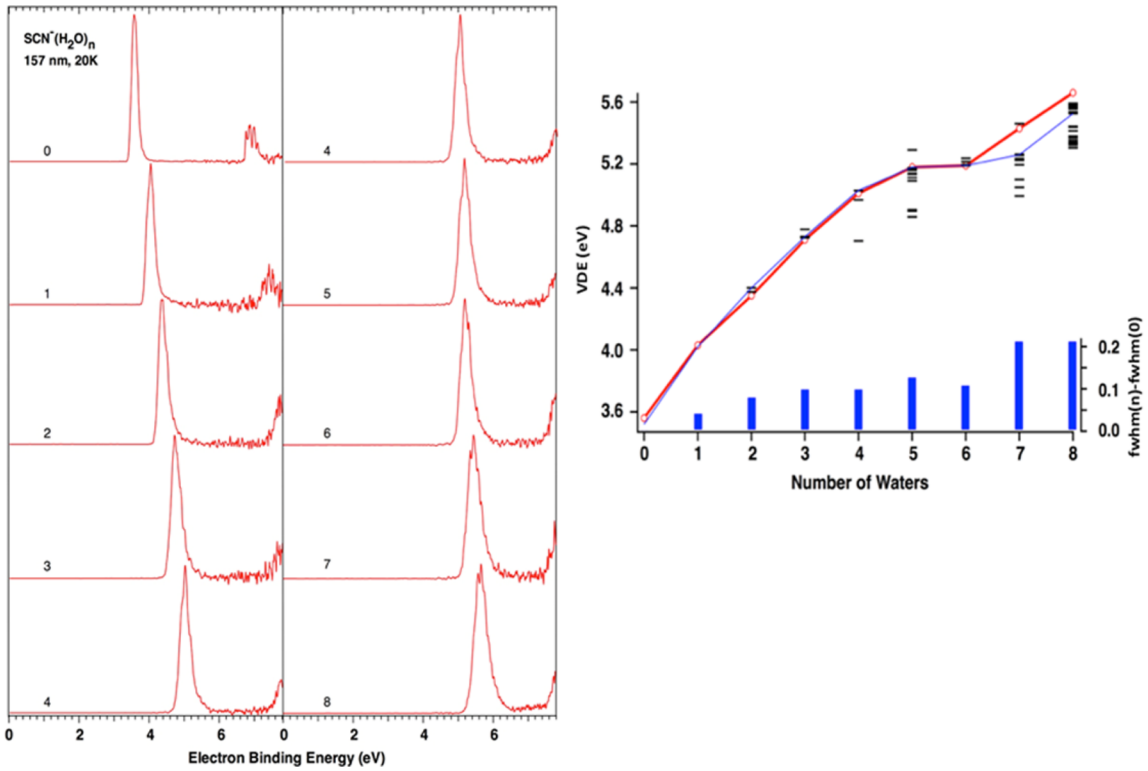

Figure 6. (Left) 20 K NIPE spectra of $SCN^-(H_2O)_n$, n = 0−8, at 157 nm (7.867 eV). (Right) Vertical detachment energies (VDEs) of the SCN^- water cluster. Experimental data are shown by a red line with circle markers. VDE values for the lowest energy calculated clusters are shown by a thin blue line. Calculated VDE values for all the clusters within 1.2 kcal/mol of the lowest energy clusters are also shown using horizontal bars. The full widths at half-maximum (fwhm) of $SCN^-(H_2O)_n$ relative to that of SCN^- are displayed as vertical blue bars. Reproduced from ref 32 with permission from the American Chemical Society.

This expression shows that $\Delta EBE(n) < 0$ would manifest itself in the anomalous decrease if $\Delta E^{neutr}(n) < \Delta E^{anion}(n)$ (i.e., $\Delta E^{neutr}(n)$ more negative than $\Delta E^{anion}(n)$). This is precisely the situation displayed in the analysis of computed cluster energy differences, shown as a function of cluster size in Figure 5b. As the cluster grows, the energy differences for the anion state diminish in magnitude due to charge screening effects, exhibiting only small variations. The neutral state experiences much

DOI: 10.1021/acs.jpca.6b09784
J. Phys. Chem. A 2017, 121, 1389−1401

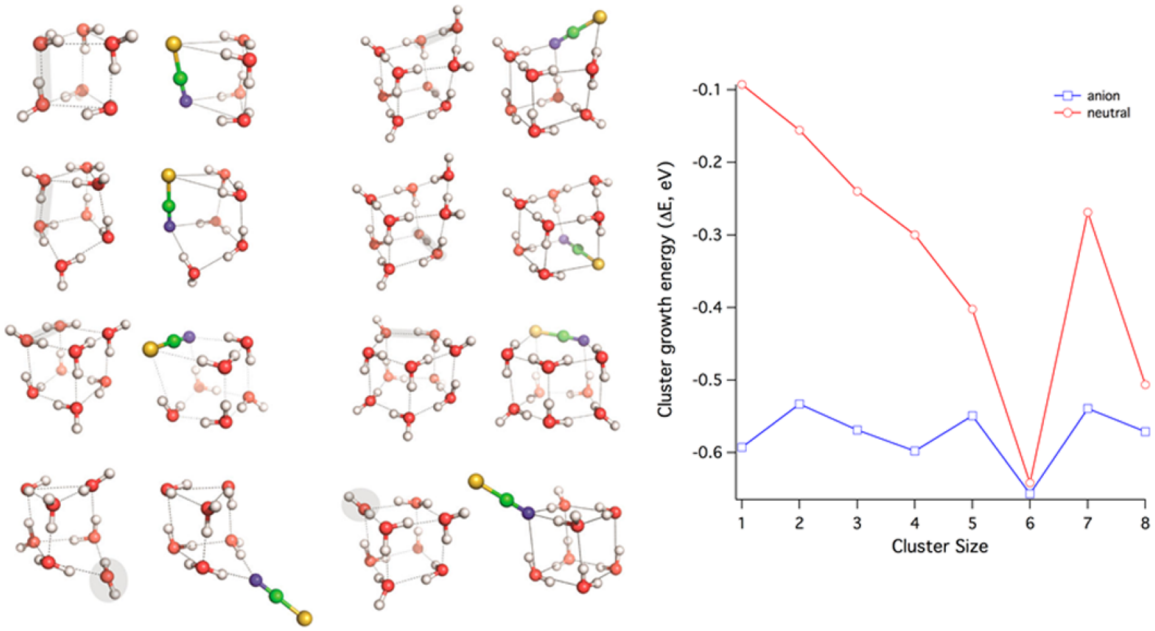

Figure 7. (Left) Comparison between selected ground state and low lying isomers of SCN^- water clusters and pure water clusters. The highlighted region indicates the replacement position. (Right) Calculated water binding energies (in eV) for anion (blue) and neutral (red) SCN water clusters as a function of cluster size. The reference energy of water was set at −76.43413 au. Reproduced from ref 32 with permission from the American Chemical Society.

larger fluctuations, confirming its "sensitivity" to the structure of the solvent. Consistent with the argument given above, the energy of the neutral state experiences a sudden drop at $n = 10$, suggesting a transition to a solvent structure highly favorable for the neutral $IO_3^•$ solute. This is also the first point where the neutral energy difference curve goes below the anion curve; i.e., the 10th water molecule binds stronger in the neutral than in the anionic state to the $n = 9$ clusters at the given anionic cluster structures. Further analysis indicates the angle (θ) between the iodate C_{3v} axis and the solvent electric field at the iodate center of mass provides a good description for the admittedly nonuniform case of iodate water clusters. As shown in Figure 5, there is a good correlation between the angle θ and the neutral cluster energy differences.

Hydrated neutral clusters are expected to be very different from their ionic counterparts where the dominant charge (monopole) field is absent. Our study suggests that charge anisotropy (permanent dipole) of polar solute molecules plays an important role in selecting favorable solvent network configurations, and consequently influencing their chemical reactivity and physical properties. The rationale of preferred specific solvation structures based on a simple geometrical argument between the solute C_{3v} symmetry axis and the solvent-network electric field is conceptually simple and provides a new way of understanding structures and properties of complex molecules in aqueous environments, including ubiquitous zwitterions of biological molecules.

3.2. $SCN^-(H_2O)_n$ ($n = 0–8$) Clusters: A Chaotrope Case. As a comparison, we also combined experimental photoelectron spectroscopy measurements with theoretical modeling to examine the evolution of solvation structure up to eight waters for the *chaotrope* SCN^- anion.[32] Figure 6 displays the $T = 20$ K NIPE spectra of $SCN^-(H_2O)_n$ ($n = 0–8$) at 157 nm, showing a steadily stepwise blue shift in EBE for $n = 0–5$ as expected, a surprise identical EBE for $n = 6$ compared to that of $n = 5$, followed by a continuous blue shift in energy for $n = 7$ and 8. Close examination of all spectra unravels an interesting variation on the spectral bandwidth (full width at half-maximum, fwhm) with addition of each water molecule: the fwhm(n) of $SCN^-(H_2O)_n$ shows a gradual increase from $n = 0$ to 5, but a sudden decrease at $n = 6$, followed by appreciable increases for $n = 7$ and 8 (Figure 6). In general, the spectral bands of clusters are expected to get broader with the addition of each water molecule due to the extra solvent coordinates introduced in the cluster anions and possible coexistence of multiple isomers. It is certainly unexpected to see a drop of spectral bandwidth at $n = 6$ from $n = 5$. Thus, our NIPES study seems to suggest $SCN^-(H_2O)_6$ with a special trait en route solvation evolution, which is born out from our theoretical calculations that show $SCN^-(H_2O)_6$ forms an almost perfect cubic structure with a special stability (Figure 7).

We found a distinctly different solvation motif of SCN^- compared to IO_3^-. We observed that SCN^- indeed fits the description of a weakly hydrated ion and its solvation is heavily driven by stabilization of the water−water interaction network. However, the impact on water structure is more subtle than that associated with typical "structure breakers". In particular, we observe that the solvation structure of SCN^- preserves the "packing" arrangement of the water network but changes local directionality of hydrogen bonds in the local solvent region. The resulting effect is closer to that of a "*structure weakener*" instead of "*structure breaker*", where a solute can be readily accommodated into the native water network by replacing a single water molecule in the corner or by substituting a water dimer on the edge, at the cost of compromising stability due to constraints on hydrogen bonding directionality (Figure 7).

Further insight into the interplay between solute−solvent and solvent−solvent stabilization effects can be gained from the analysis of cluster growth energy, $\Delta E(n) = E(n) - E(n-1) - E_w$, which is the difference between total energy of n and $n-1$ clusters referenced to the energy of the single water molecule (E_w) (eq 1). Of particular interest is the behavior of $\Delta E(n)$ for

DOI: 10.1021/acs.jpca.6b09784
J. Phys. Chem. A 2017, 121, 1389−1401

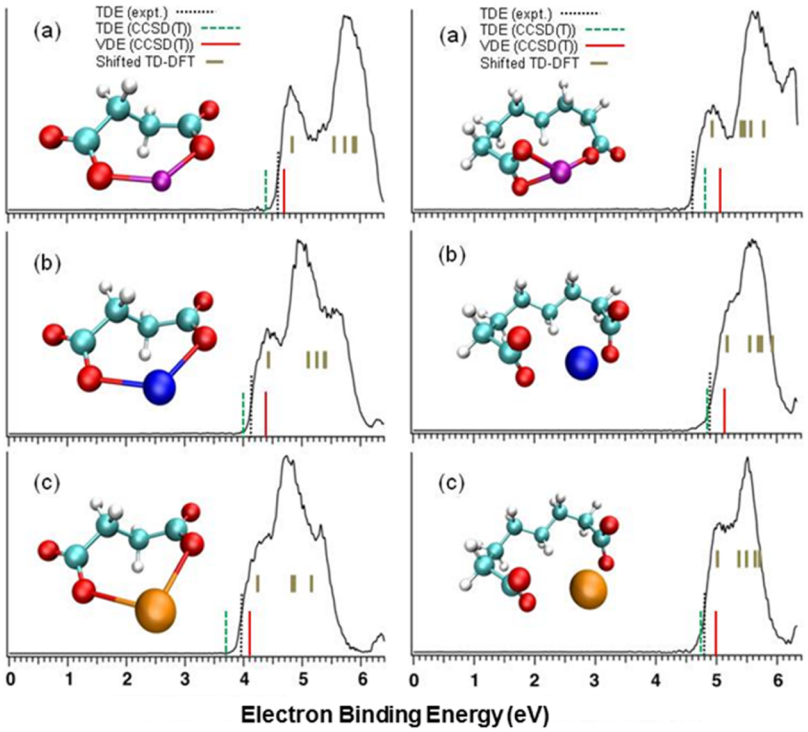

Figure 8. Low temperature 193 nm (6.424 eV) photoelectron spectra of $M^+{-}{}^-O_2C(CH_2)_nCO_2^-$ for n = 2 (left) and 6 (right), M = Li (a), Na (b), and K (c). The B3LYP/6-311++G** optimized structures of the anions are shown. The calculated TDE and VDE as well as the shifted TD-DFT results are compared with the spectra. Reproduced from ref 34 with permission from the American Chemical Society.

the neutral system ($\Delta E^{neutr}(n)$), where reduction in solute–water interactions allows us to expose the contribution from internal water network. As Figure 7 shows, $\Delta E^{neutr}(n)$ steadily gains in (negative) value reaching the peak at n = 6 cluster. This is in contrast to the behavior observed for the iodate solvation, where $\Delta E^{neutr}(n)$ shows an oscillatory behavior stemming from directional solute dipole water interactions.[31] This strongly suggests that the growth of the solvated cluster in the SCN case is accompanied by steady stabilization of the internal water network. The fact that this contribution peaks at the n = 6 case indicates that the cubic structure achieved in this case represents a particular stable water configuration. This is consistent with the particularly large calculated band gap for the n = 6 case and reduced experimental spectral width (Figure 6). The enhanced stabilization of the water network in the n = 6 cluster also explains a peculiar flattening of the experimental VDE value across the n = 5 and n = 6 clusters. Indeed, this would imply that overall cluster stabilization for the n = 6 case is derived from the solvent part of the systems, but not the solute–solvent stabilization effects that would be reflected in the increased value of VDE values. It is also interesting to note that the stepwise cluster energy for SCN^-, $\Delta E^{anion}(n)$, remains largely constant for n = 1–8, because, as a chaotrope, SCN^- always resides at either the edge or corner of native water clusters. This behavior is distinctly different from the kosmotrope IO_3^-, where the absolute value of $\Delta E^{anion}(n)$ gradually reduced with number of waters as a result of charge screening effects due to stronger solute–solvent interactions in the smaller clusters and reorganizing ability for local water molecules by the solute.

3.3. Other Hofmeister Anion Solvation. The insights from the above studies on the structural evolution of the kosmotrope IO_3^- vs chaotrope SCN^- anion–water clusters appear to be applicable to other anion–water solvation. For instance, as a prototypical kosmotrope anion, sulfate (SO_4^{2-}) has shown its strong ability to organize water molecules by breaking water–water hydrogen bonds and forming anion–water hydrogen bonds,[51,59,60] even to be able to pattern water molecules beyond its immediate solvation shells[61] due to much stronger anion–water interaction. On the contrary, our recent work on bicarbonate (HCO_3^-)–water clusters[33] shows that bicarbonate is always at the exterior of the hydrated clusters with a plethora of intact water–water network, suggesting that it lacks the ability to order water molecules because of comparable solute–solvent and solvent–solvent interactions.

4. ANION SPECIFICITY IN ION RECOGNITION AND ANION–π COMPLEXES

Anion specificity is widely observed, not only in aqueous solutions as described in section 3 but also in molecular recognition and selectivity that plays an essential role and has been exploited in many diverse fields from life processes[62,63] to material design and rational synthesis.[64,65] In this section, we present our recent studies using cluster models to investigate anion specific effects in ion-pair and anion–π complexes, as well as explore hydrogen bonding network and its implication on molecular recognition in guest–host chemistry.

4.1. Study of Ion-Pair Specific Interactions: Alkali Cations with Dicarboxylate Dianions. The ion-pair interaction between alkali metal cations, M^+, and carboxylate has been a topic of interest, partly driven by the important biological implications of the remarkable metal selectivity (Na^+ versus K^+ ion channels) present in the normal functioning of life.[62,63] A better understanding of such interactions is also important in modeling ion–biomolecule interactions in solutions that involve electrolytes, which often show profound ion specificity.[53−55] We reported a direct probe of interactions

DOI: 10.1021/acs.jpca.6b09784
J. Phys. Chem. A 2017, 121, 1389−1401

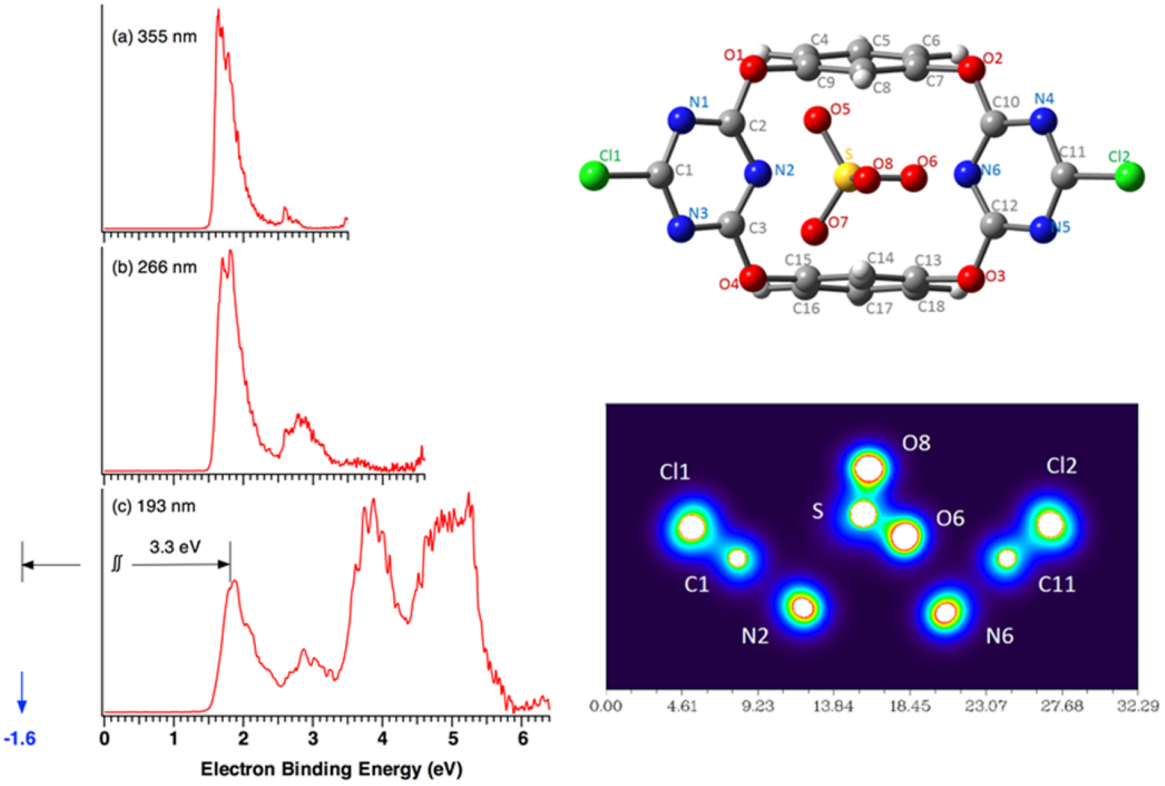

Figure 9. (Left) Low temperature negative ion photoelectron spectra of $\mathbf{1}\cdot SO_4^{2-}$ at 355 (a), 266 (b) and 193 nm (c). The blue arrow indicates the electron binding energy of the sulfate free dianion. The increase in the electron binding energy of sulfate upon associating with **1** provides a rough estimate of the sulfate-π interaction strength. (Right) Top view of the optimized structure of $\mathbf{1}\cdot SO_4^{2-}$ (top); and side view of electron density of the anion-arene complex (bottom). Adapted from ref 35 with permission from the PCCP Owner Societies. Copyright 2015.

between M^+ and dicarboxylate dianions, $^-O_2C(CH_2)_nCO_2^-$ (DC_n^{2-}), in the gas phase by combining NIPES and ab initio electronic structure calculations on nine $M^+-DC_n^{2-}$ complexes (M = Li, Na, K; n = 2, 4, 6).[34] This allowed us to investigate how the aliphatic length $(CH_2)_n$, flexibility of the dianions, and the size of cations influence these ion-pair cluster structures. The NIPE spectra presented in Figure 8 show that the electron binding energy decreases in the order of $Li^+ > Na^+ > K^+$ for complexes of $M^+-DC_2^{2-}$, whereas the order is changed to $Li^+ < Na^+ \approx K^+$ when M^+ interacts with a more flexible DC_6^{2-} dianion. Theoretical modeling suggests that M^+ prefers to interact with both ends of the carboxylate $-COO^-$ groups by bending the flexible aliphatic backbone, and the local binding environments are found to depend upon backbone length n, carboxylate orientation, and the specific cation M^+. The observed variation of EBEs reflects how well each specific dicarboxylate dianion accommodates each M^+, demonstrating the delicate interplay among several factors (electrostatic interaction, size matching, and strain energy) that play critical roles in determining the structures and energetics of gaseous clusters as well as ion specificity and selectivity in solutions and biological systems.

4.2. Molecular Level Probe of Anion–π Specific Interactions. Proposed in theory and confirmed experimentally, anion–π interactions have been recognized as new and important noncovalent binding forces.[64,65] Despite extensive theoretical studies, numerous crystal structure identifications, and a plethora of solution-phase investigations, anion–π interaction strengths that are free from complications of condensed-phase environments have not been directly measured. We conducted a joint photoelectron spectroscopic and theoretical study on this subject, in which tetraoxacalix[2]arene[2]triazine **1**, an electron-deficient and cavity self-tunable macrocyclic molecule (Figure 9), was used as a charge-neutral host to probe its interactions with a series of anions with distinctly different shapes and charge states (spherical halides Cl^-, Br^-, I^-, linear thiocyanate SCN^-, trigonal planar nitrate NO_3^-, pyramidic iodate IO_3^-, and tetrahedral sulfate SO_4^{2-}).[35] The electron binding energies of the resultant gaseous 1:1 complexes ($\mathbf{1}\cdot Cl^-$, $\mathbf{1}\cdot Br^-$, $\mathbf{1}\cdot I^-$, $\mathbf{1}\cdot SCN^-$, $\mathbf{1}\cdot NO_3^-$, $\mathbf{1}\cdot IO_3^-$, and $\mathbf{1}\cdot SO_4^{2-}$) were directly measured experimentally, exhibiting substantial noncovalent interactions with pronounced anion specific effects. The binding strengths between Cl^-, NO_3^-, IO_3^-, and **1** are found to be strongest among all singly charged anions, amounting to ca. 30 kcal/mol, but only about 40% of that between **1** and SO_4^{2-}. Quantum chemical calculations reveal that all anions reside in the center of the cavity of **1** with anion–π binding motif in the complexes' optimized structures, where **1** is seen to be able to self-regulate its cavity structure to accommodate anions of different geometries and three-dimensional shapes. Electron density surface and charge distribution analyses further support anion–π binding (Figure 9). The calculated binding energies of the anions and **1** nicely reproduce the experimentally estimated electron binding energy increases. The conclusion derived from our gas-phase study correlates well with the solution-phase measurement,[66] illustrating that size-selective photoelectron spectroscopy combined with theoretical calculations represents a powerful technique to probe anion–π interactions with the potential to provide quantitative guest–host molecular binding strengths and unravel fundamental insights in specific anion recognition.

4.3. Hydrogen Bond Network and Its Implications in Anion Recognition. Hydrogen bonds are ubiquitous in

DOI: 10.1021/acs.jpca.6b09784
J. Phys. Chem. A 2017, 121, 1389–1401

nature and are important in many fields, including supramolecular, biological, and medicinal systems,[67−69] as well as atmospheric chemistry.[40,70−73] Hydrogen bond networks (HBN) have been proposed to play crucial roles in enzymatic reactions, in which many enzymes catalyze a wide variety of chemical processes by using two or even three hydrogen bonds to a single oxygen atom in what is commonly referred to as an oxyanion hole. The energies of these hydrogen bonding interactions are important in catalysis and ion recognition but are not well understood. This issue has been addressed by Steven Kass of University of Minnesota employing a combination of approaches including synthesis of various model compounds, solution-phase association constant measurements, gas-phase infrared action spectroscopy, and ab initio computations and has been examined via ESI-NIPES as well in collaboration with my group.[36−39] For an example, a series of polyhydroxyalcohols (i.e., polyols) were synthesized, and their monodeprotonated anions were proposed to mimic a bound oxyanion hole HBN with variable hydrogen bonds (Figure 10).

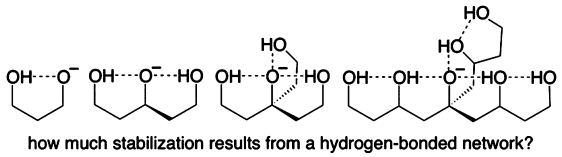

Figure 10. Series of polyols that have been studied using NIPES to provide quantitative measures of H-bond strength. Reproduced from ref 36 with permission from the American Chemical Society.

We examined these anions via ESI-NIPES and computations to directly probe the energetic consequences of hydrogen bond arrays formed on the oxygen anion hole[36] and found that the strength of the hydrogen bond arrays systematically increases with the number of hydroxyl groups from 1 to 3 and for 6. That is, an oxygen anion center is stabilized most effectively by up to 3 hydrogen bond donors, but in the process the donor groups become better hydrogen bond acceptors. The resulting hydrogen-bonded network can provide a large energetic stabilization, i.e., 47 and 64 kcal/mol with 3 and 6 hydrogen bonds, respectively, that may lead to catalytic rate enhancements and greater acidities and basicities than those measured in water. In addition, ESI-NIPES was applied to directly probe the energetic consequences of the binding abilities of various polyols to a number of anions: for example, Cl^- in Figure 11, in charactering the cooperative effects of HBN and its effects on selective anion recognition.[37−39]

5. CLUSTER MODEL STUDIES ON SPECIFIC MOLECULAR EFFECTS IN AEROSOL PARTICLE FORMATION

One of our major research directions is to gain molecular level understanding of aerosol formation processes,[70−73] which have significant impacts on new particle formation occurred under diverse pristine and polluted environments with profound implications on human health and climate.[74,75] Owing to the limitation of experimental field measurements, much of the research on this subject has been so far focused on large particle sizes (>3 nm).[71,73] Theoretical analysis performed using classical nucleation theory is geared toward a macroscopic description based on liquid drop theory.[72] And the kinetic extensions of the nucleation theorem on the basis of the first-principles have been adopted in the investigation of the

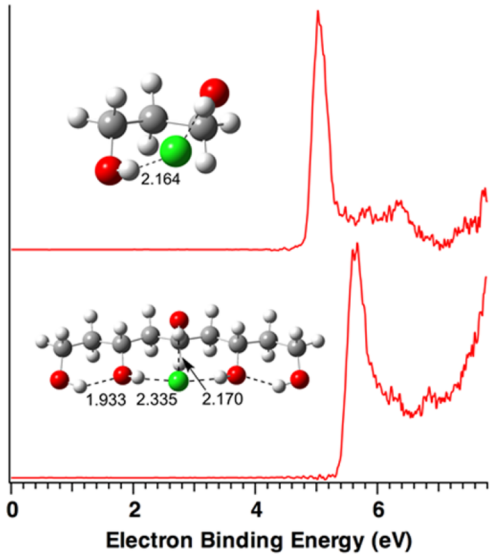

Figure 11. Low temperature (12 K) photoelectron spectra of diol- and pentaol-chloride complexes at 157 nm. The electron binding energy of the latter is significantly larger than the former due to one extra direct H-bond and two secondary H-bonds available in the pentaol complex as shown in their respective M06-2X/aug-cc-pVTZ structures (inset). Adapted from ref 39 with permission from the American Chemical Society.

nucleation problem.[76,77] Nevertheless, the more microscopic, molecular level, investigations have been fairly limited in scope, but their importance is steadily increasing.[40,72] Such analysis may play an important role in understanding specific molecular effects that have been implicated in aerosol formation in the marine boundary layer. Molecular level information also forms a necessary prerequisite for better model parameters for macroscopic analysis.[72]

A complementary way to investigate these issues, especially at the molecular scale, can be found in the analysis of clusters with tunable compositions and sizes.[40−42,72,78−80] The development in this area has been so far mostly dominated by theoretical studies, which have provided useful information on the small clusters formed by atmospheric nucleation precursors consisting of a series of small organic species with sulfuric acid and/or water to investigate how organic acids enhance aerosol formation and growth.[78,79,81−85] In addition to theoretical studies, several atmospherically relevant clusters consisting of sulfuric acid/bisulfate, nitric acid/nitrate, NH_3/amine, and H_2O have been investigated using infrared photodissociation spectroscopy (IRPD),[7−9] collision induced dissociation (CID),[10] and mass spectrometry.[11−13] Our cluster study addresses these important issues through integrated ESI-NIPES experiments and computational approaches. This involves synthesis of size selected particle clusters of atmospherically relevant compositions, NIPES measurements, and theoretical analysis based on accurate ab initio calculations.[40−42] Our objective is to provide a comprehensive molecular level characterization of common multicomponent aerosol particles, as well as to gain a fundamental understating of molecular specific effects and the energetics that drive their formation.

5.1. Negative Ion Photoelectron Spectroscopy Study of Atmospherically Related Clusters and Species. Recent lab and field measurements have indicated critical roles of organic acids in enhancing new atmospheric aerosol formation.[86,87] Such findings have stimulated theoretical and experimental

DOI: 10.1021/acs.jpca.6b09784
J. Phys. Chem. A 2017, 121, 1389−1401

studies with the aim of understanding the interaction of organic acids with common aerosol nucleation precursors, like bisulfate (HSO_4^-). We carried out a combined negative ion photoelectron spectroscopic and theoretical investigation of molecular clusters formed by HSO_4^- with succinic acid ($HO_2C(CH_2)_2CO_2H$) along with $HSO_4^-(H_2O)_n$ and $HSO_4^-(H_2SO_4)_n$.[40] As shown in Figure 12, it was found that one SUA molecule can stabilize

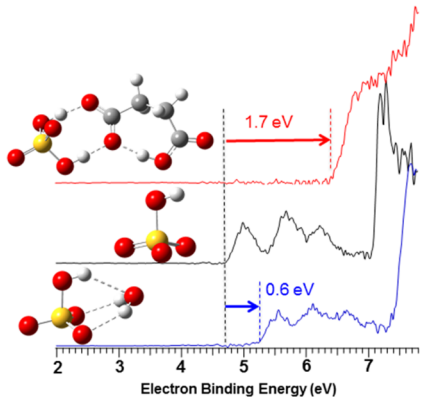

Figure 12. Negative ion photoelectron spectroscopy reveals the electron binding energy of bisulfate with succinic acid is roughly three times stronger than with water. Reproduced from ref 40 with permission from the American Chemical Society.

HSO_4^- by ca. 39 kcal/mol in electron binding energy (which is equal roughly to the molecular binding energy between these two molecules), triple the corresponding value that one water molecule is capable of (ca. 13 kcal/mol), thus providing direct experimental evidence showing a significant thermodynamic advantage by involving organic acid molecules to promote formation and growth in bisulfate clusters and aerosols.

Organic acids also represent an important component of atmospheric aerosols and have been found in abundance in a variety of urban, rural, and marine environments.[88−90] Their significance in new particle formation and nucleation is supported by substantial experimental evidence.[72,78] One of the particularly important questions is the role they play during the initial stage of aerosol particles formation. We have recently studied properties of dicarboxylic acid homodimer complexes, $HO_2C(CH_2)_nCO_2^-[HO_2C(CH_2)_nCO_2H]$, n = 0−12, as potentially important intermediates in aerosol formation processes.[41] These results are analyzed with quantum-mechanical calculations, which provide further information about equilibrium structures, thermochemical parameters associated with the complex formation, and evaporation rates. We find that upon formation of the dimer complexes, the electron binding energies increase by 1.3−1.7 eV (30.0−39.2 kcal/mol), indicating increased stability of the dimerized complexes. Calculations indicate that these dimer complexes are characterized by the presence of strong intermolecular hydrogen bonds with high binding energies, and are thermodynamically favorable to form with low evaporation rates. By comparison to the previous study of the $HSO_4^-[HO_2C(CH_2)_2CO_2H]$ complex,[40] it has been shown that $HO_2C(CH_2)_2CO_2^-[HO_2C(CH_2)_2CO_2H]$ has very similar thermochemical properties. These results imply that dicarboxylic acids not only contribute to the heterogeneous complexes formation involving sulfuric acid and dicarboxylic acids but also can promote the formation of homogeneous complexes by involving dicarboxylic acids themselves.

5.2. Probing the Early Stages of Solvation of *cis*-Pinate Dianions. *cis*-Pinic acid is one of the most important oxidation products formed from ozonolysis of α-pinene[91]—a key monoterpene compound in biogenic emission processes.[92] Molecular level understanding of its interaction with water in cluster formation is an important and necessary prerequisite toward ascertaining its role in the aerosol formation processes. We studied the structures and energetics of the solvated clusters of *cis*-pinate (*cis*-PA^{2-}), the doubly deprotonated dicarboxylate of *cis*-pinic acid, with H_2O, CH_3OH, and CH_3CN by negative ion photoelectron spectroscopy and *ab initio* theoretical calculations.[42] We found that *cis*-PA^{2-} prefers being solvated alternately on the two $-CO_2^-$ groups with an increase of solvent coverage, a well-known solvation pattern that has been observed in microhydrated linear dicarboxylate dianion (DC_n^{2-}) clusters.[93] Experiments and calculations further reveal an intriguing feature for the existence of the asymmetric type isomers for *cis*-$PA^{2-}(H_2O)_2$ and *cis*-$PA^{2-}(CH_3OH)_2$, in which both solvent molecules interact with only one of the $-CO_2^-$ groups—a phenomena that has not been observed in DC_n^{2-} water clusters and exhibits the subtle effect of the rigid four-membered carbon ring brought in on the *cis*-PA^{2-} solvation (Figure 13). The dominant interactions between *cis*-PA^{2-} and

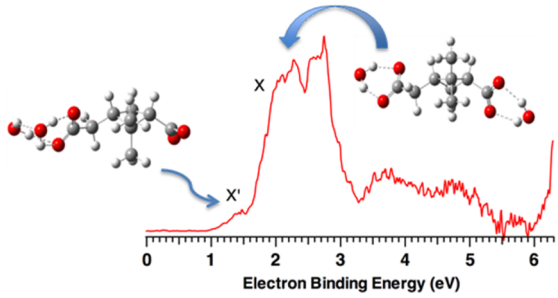

Figure 13. Integrated theoretical calculation and negative ion photoelectron spectroscopy study allows specific solvation structures of *cis*-pinic acid to be determined. Reproduced from ref 42 with permission from the PCCP Owner Societies. Copyright 2016.

solvent molecules form bidentate $O^-\cdots H-O$ H-bonds for H_2O, $O^-\cdots H-O$, and $O^-\cdots H-C$ H-bonds for CH_3OH, and tridentate $O^-\cdots H-C$ H-bonds for CH_3CN. The formation of intersolvent H-bonds between H_2O and CH_3CN is found to be favorable in mixed solvent clusters, different from that between H_2O and CH_3OH. These findings have important implications for understanding the mechanism of cluster growth and formation of atmospheric organic aerosols, as well as for rationalizing the nature of structure−function relationship of proteins containing carboxylate groups under various solvent environments.

6. FUTURE PERSPECTIVES

Condensed-phase and interfacial chemical physics, at first glance, is a subject full of complexity, often described in terms of macroscopic cause-and-effect languages. Yet it can be often reduced to, or at least largely to, a local process, in which related molecules interact resulting in the macroscopically observed phenomena with the rest of the environment as "a passive reaction medium". Therefore, obtaining molecular-level understanding of molecular interactions among molecules and reactive species within local regions (active sites) remains the key to understanding and controlling these processes. In this regard, clusters with a controlled number of solvent molecules

DOI: 10.1021/acs.jpca.6b09784
J. Phys. Chem. A 2017, 121, 1389−1401

and molecular specificity represent ideal model systems to mimic the multicomponent and multiphase complex nature of chemical and physical processes in bulk solutions and at interfaces with promising bridge molecular description and macroscopic observations. The experimental capabilities that we have developed, i.e., temperature-controlled ESI-NIPES of size-selective clusters, give us opportunities to attack a broad range of fundamental chemical physics problems pertinent to ionic solvation and solution chemistry. Our cluster model studies have been shown and are expected to continue to provide important microscopic information about intrinsic electronic, geometric structures, and dynamics of varieties of clusters, redox species, and solvated anion complexes that are important to chemical transformations, biological functions, sustainable energy, and predictive material synthesis. Meanwhile, sophisticated new experimental techniques, such as isomer-selective femtosecond time-resolved photoelectron spectroscopy and angle-resolved photoelectron imaging spectroscopy with ultrafast time resolution or wavenumber energy resolution coupled with ESI source, have been developed by several other groups worldwide to investigate dynamics of MCAs and solution-phase species, as well as to probe autodetachment vs internal conversion processes after resonant excitations.[30,94−97]

One of our future studies will be investigation of microsolvation of environmentally important anions at well-controlled and variable temperatures to elucidating the underlying entropic effects[49] and large amplitude motions involving the structures with the doubly and singly H-bonded water molecules in the solvation of complex anions.[42] We would like to build up complexity by adding composition (from binary to ternary and quaternary) and extending the cluster size range (from small and medium size to large clusters containing 50−100 solvent molecules)[61,98] to make these clusters better model systems to mimic the multicomponent, multiphase, and complex nature of chemical and physical processes occurred in bulk solutions and at interfaces. For instance, extending our previous studies of binary alkali metal cation dicarboxylate complexes $(M^+{\cdot}DC_n^{2-})$[34] to ternary clusters of $(M^+{\cdot}DC_n^{2-})(H_2O)_m$ by adding water molecules would provide an excellent parameter space to examine direct ion-pair and ion−water interactions. Molecular dynamics simulations and a theoretical structural search based on unbiased methods[33] are needed to illustrate the delicate interplay among direct ion-pair, solute−water, and water−water interactions that determine the energetics, binding motifs, and structures of these model systems. In a similar vein, clusters containing Hofmesiter ions and proteins/peptides provide well-defined systems to investigate the molecular mechanisms of ion-specific effects on proteins/peptides, focused on finding ion specific binding sites and intermolecular interactions between macromolecules and ions,[99,100] and between ions and water in the immediate vicinity of ions. The obtained spectroscopic data, theoretical modeling, and in-depth analysis of different intermolecular interactions will help to provide a molecular level understanding of ion specific effects in the Hofmeister series that was initially discovered in aqueous protein solutions by adding different salts. It is also related to anion recognition and ion selectivity[34−39] that are important concepts in biological function and material science.

Although atmospheric field measurements have identified sulfuric acid including the bisulfate ion as a key nucleation precursor, nucleation rates inferred from the two well established binary $(H_2SO_4{-}H_2O)$ or ternary $(H_2SO_4{-}H_2O{-}NH_3)$ mechanisms cannot explain the observed nucleation rates obtained from field measurements.[72] Other species, such as amines and organic compounds, which may enhance new particle formation, have been introduced by recent laboratory and field studies to account for the discrepancies.[72,86] Future direction will be focused on more complex systems involving organic matter, amines, sulfuric acid, water, and sea salts to experimentally identify key molecular components in promoting aerosol formation, to provide a molecular description of the early stages of nucleation processes, and to obtain quantitative thermodynamic parameters accounting for the formation of atmospherically relevant clusters.

AUTHOR INFORMATION

Corresponding Author

*E-mail: xuebin.wang@pnnl.gov.

ORCID

Xue-Bin Wang: 0000-0001-8326-1780

Notes

The author declares no competing financial interest.

Biography

Xue-Bin Wang received his B.S. in Chemical Physics from University of Science and Technology of China (1988) and his Ph.D in Physical Chemistry from the Institute of Chemistry, Chinese Academy of Sciences (1995), under the supervision of Qihe Zhu. He worked as a visiting graduate student under the guidance of R. D. Levine from 1993 to 1995 in Hebrew University of Jerusalem. He joined R. Bersohn's group in 1995 at Columbia University, and L.-S. Wang's group in 1997 at PNNL/Washington State University as postdoctoral research associate. He worked at PNNL/Washington State University as research scientist and associate research professor from 2000 to 2011. He formally joined PNNL in 2011 and is currently a senior research scientist in the Physical Sciences Division at PNNL.

ACKNOWLEDGMENTS

I thank Steven R. Kass, Western T. Borden, Marat Valiev, Sotiris S. Xantheas, and Shawn Kathmann for the role that each of them played in furthering the scientific research described in this paper. I am indebted to my colleagues Niranjan Govind and Karol Kowalski who have always been very enthusiastic in carrying out computational studies and providing scientific insights. I thank my longtime colleague, Prof. Lai-Sheng Wang, whom I worked for and collaborated with for many years. I am profoundly grateful to my group members, including postdoctoral research associates − Drs. Shihu Deng, Gao-Lei Hou, Zheng Yang, visiting scholars and students − Hui Wen, Jian

DOI: 10.1021/acs.jpca.6b09784
J. Phys. Chem. A 2017, 121, 1389−1401

Zhang, Xiang-Yu Kong, Zhengbo Qin, who have contributed to the research discussed in this article. The experimental work presented here was supported by the U.S. Department of Energy (DOE), Office of Science, Office of Basic Energy Sciences, the Division of Chemical Sciences, Geosciences and Biosciences, and was performed using EMSL, a national scientific user facility sponsored by DOE's Office of Biological and Environmental Research and located at Pacific Northwest National Laboratory, which is operated by Battelle Memorial Institute for the DOE.

REFERENCES

(1) Tobias, D. J.; Hemminger, J. C. Getting Specific About Specific Ion Effects. *Science* **2008**, *319*, 1197−1198.
(2) Knipping, E. M.; Lakin, M. J.; Foster, K. L.; Jungwirth, P.; Tobias, D. J.; Gerber, R. B.; Dabdub, D.; Finlayson-Pitts, B. J. Experiments and Simulations of Ion-Enhanced Interfacial Chemistry on Aqueous Nacl Aerosols. *Science* **2000**, *288*, 301−306.
(3) Dedonder-Lardeux, C.; Grégoire, G.; Jouvet, C.; Martrenchard, S.; Solgadi, D. Charge Separation in Molecular Clusters: Dissolution of a Salt in a Salt−(Solvent)n Cluster. *Chem. Rev.* **2000**, *100*, 4023−4038.
(4) Li, R.-Z.; Liu, C.-W.; Gao, Y. Q.; Jiang, H.; Xu, H.-G.; Zheng, W.-J. Microsolvation of LiIand CsI in Water: Anion Photoelectron Spectroscopy and Ab Initio Calculations. *J. Am. Chem. Soc.* **2013**, *135*, 5190−5199.
(5) Asmis, K. R.; Neumark, D. M. Vibrational Spectroscopy of Microhydrated Conjugate Base Anions. *Acc. Chem. Res.* **2012**, *45*, 43−52.
(6) Li, X.; Wang, H.; Bowen, K. H. Photoelectron Spectroscopic Study of the Hydrated Nucleoside Anions: Uridine$^-(H_2O)_{n=0-2}$, Cytidine$^-(H_2O)_{n=0-2}$, and Thymidine$^-(H_2O)_{n=0,1}$. *J. Chem. Phys.* **2010**, *133*, 144304.
(7) Yacovitch, T. I.; Wende, T.; Jiang, L.; Heine, N.; Meijer, G.; Neumark, D. M.; Asmis, K. R. Infrared Spectroscopy of Hydrated Bisulfate Anion Clusters: $HSO_4^-(H_2O)_{1-16}$. *J. Phys. Chem. Lett.* **2011**, *2*, 2135−2140.
(8) Yacovitch, T. I.; Heine, N.; Brieger, C.; Wende, T.; Hock, C.; Neumark, D. M.; Asmis, K. R. Communication: Vibrational Spectroscopy of Atmospherically Relevant Acid Cluster Anions: Bisulfate versus Nitrate Core Structures. *J. Chem. Phys.* **2012**, *136*, 241102.
(9) Johnson, C. J.; Johnson, M. A. Vibrational Spectra and Fragmentation Pathways of Size-Selected, D_2-Tagged Ammonium/Methylammonium Bisulfate Clusters. *J. Phys. Chem. A* **2013**, *117*, 13265−13274.
(10) Bzdek, B. R.; DePalma, J. W.; Ridge, D. P.; Laskin, J.; Johnston, M. V. Fragmentation Energetics of Clusters Relevant to Atmospheric New Particle Formation. *J. Am. Chem. Soc.* **2013**, *135*, 3276−3285.
(11) Zatula, A. S.; Andersson, P. U.; Ryding, M. J.; Uggerud, E. Proton Mobility and Stability of Water Clusters Containing the Bisulfate Anion, $HSO_4^-(H_2O)_n$. *Phys. Chem. Chem. Phys.* **2011**, *13*, 13287−13294.
(12) Bush, M. F.; Saykally, R. J.; Williams, E. R. Evidence for Water Rings in the Hexahydrated Sulfate Dianion from IR Spectroscopy. *J. Am. Chem. Soc.* **2007**, *129*, 2220−2221.
(13) Dribinski, V.; Barbera, J.; Martin, J. P.; Svendsen, A.; Thompson, M. A.; Parson, R.; Lineberger, W. C. Time-Resolved Study of Solvent-Induced Recombination in Photodissociated $IBr^-(CO_2)_n$ Clusters. *J. Chem. Phys.* **2006**, *125*, 133405.
(14) Lovejoy, E. R.; Curtius, J. Cluster Ion Thermal Decomposition (II): Master Equation Modeling in the Low-Pressure Limit and Fall-Off Regions. Bond Energies for $HSO_4^-(H_2SO_4)_x(HNO_3)_y$. *J. Phys. Chem. A* **2001**, *105*, 10874−10883.
(15) Robertson, W. H.; Johnson, M. A. Molecular Aspects of Halide Ion Hydration: The Cluster Approach. *Annu. Rev. Phys. Chem.* **2003**, *54*, 173−213.
(16) Hurley, S. M.; Dermota, T. E.; Hydutsky, D. P.; Castleman, A. W. Dynamics of Hydrogen Bromide Dissolution in the Ground and Excited States. *Science* **2002**, *298*, 202−204.
(17) Curtius, J.; Froyd, K. D.; Lovejoy, E. R. Cluster Ion Thermal Decomposition (I): Experimental Kinetics Study and ab Initio Calculations for $HSO_4^-(H_2SO_4)_x(HNO_3)_y$. *J. Phys. Chem. A* **2001**, *105*, 10867−10873.
(18) Weber, J. M.; Kelley, J. A.; Nielsen, S. B.; Ayotte, P.; Johnson, M. A. Isolating the Spectroscopic Signature of a Hydration Shell with the Use of Clusters: Superoxide Tetrahydrate. *Science* **2000**, *287*, 2461−2463.
(19) Duncan, M. A. Frontiers in the Spectroscopy of Mass-Selected Molecular Ions. *Int. J. Mass Spectrom.* **2000**, *200*, 545−569.
(20) Cabarcos, O. M.; Weinheimer, C. J.; Lisy, J. M.; Xantheas, S. S. Microscopic Hydration of the Fluoride Anion. *J. Chem. Phys.* **1999**, *110*, 5−8.
(21) Lisy, J. M. Spectroscopy and Structure of Solvated Alkali-Metal Ions. *Int. Rev. Phys. Chem.* **1997**, *16*, 267−289.
(22) Markovich, G.; Pollack, S.; Giniger, R.; Cheshnovsky, O. Photoelectron Spectroscopy of Cl^-, Br^-, and I^- Solvated in Water Clusters. *J. Chem. Phys.* **1994**, *101*, 9344−9353.
(23) Dang, L. X.; Garrett, B. C. Photoelectron Spectra of the Hydrated Iodine Anion from Molecular Dynamics Simulations. *J. Chem. Phys.* **1993**, *99*, 2972−2977.
(24) Wang, X.-B.; Wang, L.-S. Development of a Low-Temperature Photoelectron Spectroscopy Instrument Using an Electrospray Ion Source and a Cryogenically Controlled Ion Trap. *Rev. Sci. Instrum.* **2008**, *79*, 073108.
(25) Wang, L.-S.; Ding, C.-F.; Wang, X.-B.; Barlow, S. E. Photodetachment Photoelectron Spectroscopy of Multiply Charged Anions Using Electrospray Ionization. *Rev. Sci. Instrum.* **1999**, *70*, 1957−1966.
(26) Wang, L.-S.; Wang, X.-B. Probing Free Multiply Charged Anions Using Photodetachment Photoelectron Spectroscopy. *J. Phys. Chem. A* **2000**, *104*, 1978−1990.
(27) Dreuw, A.; Cederbaum, L. S. Multiply Charged Anions in the Gas Phase. *Chem. Rev.* **2002**, *102*, 181−200.
(28) Boxford, W. E.; Dessent, C. E. H. Probing the Intrinsic Features and Environmental Stabilization of Multiply Charged Anions. *Phys. Chem. Chem. Phys.* **2006**, *8*, 5151−5165.
(29) Wang, X.-B.; Wang, L.-S. Photoelectron Spectroscopy of Multiply Charged Anions. *Annu. Rev. Phys. Chem.* **2009**, *60*, 105−126.
(30) Wang, L.-S. Electrospray Photoelectron Spectroscopy: From Multiply-charged Anions to Ultracold Anions. *J. Chem. Phys.* **2015**, *143*, 040901.
(31) Wen, H.; Hou, G.-L.; Kathmann, S. M.; Valiev, M.; Wang, X.-B. Communication: Solute Anisotropy Effects in Hydrated Anion and Neutral Clusters. *J. Chem. Phys.* **2013**, *138*, 031101.
(32) Valiev, M.; Deng, S. H. M.; Wang, X.-B. How Anion Chaotrope Changes the Local Structure of Water: Insights from Photoelectron Spectroscopy and Theoretical Modeling of SCN− Water Clusters. *J. Phys. Chem. B* **2016**, *120*, 1518−1525.
(33) Wen, H.; Hou, G.-L.; Liu, Y.-R.; Wang, X.-B.; Huang, W. Examining the Structural Evolution of Bicarbonate-Water Clusters: Insights from Photoelectron Spectroscopy, Basin-Hopping Structural search, and Comparison with Available IR Spectral Studies. *Phys. Chem. Chem. Phys.* **2016**, *18*, 17470−17482.
(34) Murdachaew, G.; Valiev, M.; Kathmann, S. M.; Wang, X.-B. Study of Ion Specific Interactions of Alkali Cations with Dicarboxylate Dianions. *J. Phys. Chem. A* **2012**, *116*, 2055−2061.
(35) Zhang, J.; Zhou, B.; Sun, Z.-R.; Wang, X.-B. Photoelectron Spectroscopy and Theoretical Studies of Anion-π Interactions: Binding Strength and Anion Specificity. *Phys. Chem. Chem. Phys.* **2015**, *17*, 3131−3141.
(36) Shokri, A.; Schmidt, J.; Wang, X.-B.; Kass, S. R. Hydrogen Bonded Arrays: The Power of Multiple Hydrogen Bonds. *J. Am. Chem. Soc.* **2012**, *134*, 2094−2099.
(37) Shokri, A.; Schmidt, J.; Wang, X.-B.; Kass, S. R. Characterization of a Saturated and Flexible Aliphatic Polyol Anion Receptor. *J. Am. Chem. Soc.* **2012**, *134*, 16944−16947.

DOI: 10.1021/acs.jpca.6b09784
J. Phys. Chem. A 2017, 121, 1389−1401

(38) Samet, M.; Wang, X.-B.; Kass, S. R. A Preorganized Hydrogen Bond Network and Its Effect on Anion Stability. *J. Phys. Chem. A* **2014**, *118*, 5989−5993.
(39) Shokri, A.; Wang, X.-B.; Wang, Y.; O'Doherty, G. A.; Kass, S. R.Flexible acyclic polyol-chloride anion complexes and their characterization by photoelectron spectroscopy and variable temperature binding constant determinations. *J. Phys. Chem. A* **2016**, *120*, 1661−1668.
(40) Hou, G.-L.; Lin, W.; Deng, S. H. M.; Zhang, J.; Zheng, W.-J.; Paesani, F.; Wang, X.-B. Negative Ion Photoelectron Spectroscopy Reveals Thermodynamic Advantage of Organic Acids in Facilitating Formation of Bisulfate Ion Clusters: Atmospheric Implications. *J. Phys. Chem. Lett.* **2013**, *4*, 779−785.
(41) Hou, G.-L.; Valiev, M.; Wang, X.-B. Deprotonated Dicarboxylic Acid Homodimers: Hydrogen Bonds and Atmospheric Implications. *J. Phys. Chem. A* **2016**, *120*, 2342−2349.
(42) Hou, G.-L.; Kong, X.-T.; Valiev, M.; Jiang, L.; Wang, X.-B. Probing the Early Stages of Solvation of cis-Pinate Dianions by Water, Acetonitrile, and Methanol: A Photoelectron Spectroscopy and Theoretical Study. *Phys. Chem. Chem. Phys.* **2016**, *18*, 3628−3637.
(43) Guo, J. C.; Hou, G.-L.; Li, S. D.; Wang, X.-B. Probing the Low-lying Electronic States of Cyclobutanetetraone (C_4O_4) and its Radical Anion: A Low-Temperature Anion Photoelectron Spectroscopic Approach. *J. Phys. Chem. Lett.* **2012**, *3*, 304−308.
(44) Bao, X.; Hrovat, D. A.; Borden, W. T.; Wang, X.-B. Negative Ion Photoelectron Spectroscopy Confirms the Prediction that $(CO)_5$ and $(CO)_6$ Each Has a Singlet Ground State. 2013. *J. Am. Chem. Soc.* **2013**, *135*, 4291−4298.
(45) Chen, B.; Hrovat, D. A.; Deng, S. H. M.; Zhang, J.; Wang, X.-B.; Borden, W. T. The Negative Ion Photoelectron Spectrum of meta-Benzoquinone Radical Anion ($MBQ^{\bullet -}$): A Joint Experimental and Computational Study. *J. Am. Chem. Soc.* **2014**, *136*, 3589−3596.
(46) Deng, S. H. M.; Kong, X.-Y.; Zhang, G. X.; Yang, Y.; Zheng, W.-J.; Sun, Z. R.; Zhang, D.-Q.; Wang, X.-B. Vibrationally Resolved Photoelectron Spectroscopy of the Model GFP Chromophore Anion Revealing the Photoexcited S_1 State Being Both Vertically and Adiabatically Bound against the Photodetached D_0 Continuum. *J. Phys. Chem. Lett.* **2014**, *5*, 2155−2159.
(47) Wang, X.-B.; Werhahn, J. C.; Wang, L.-S.; Kowalski, K.; Laubereau, A.; Xantheas, S. S. Observation of a Remarkable Temperature Effect in the Hydrogen Bonding Structure and Dynamics of the $CN^-(H_2O)$ Cluster. *J. Phys. Chem. A* **2009**, *113*, 9579−9584.
(48) Wang, X.-B.; Kowalski, K.; Wang, L.-S.; Xantheas, S. S. Stepwise Hydration of the Cyanide Anion: A Temperature-Controlled Photoelectron Spectroscopy and Ab initio Computational Study of $CN^-(H_2O)_n$, n = 2−5. *J. Chem. Phys.* **2010**, *132*, 124306.
(49) Wang, X.-B.; Yang, J.; Wang, L.-S. Observation of Entropic Effect on Conformation Changes of Complex Systems under Well-Controlled Temperature Conditions. *J. Phys. Chem. A* **2008**, *112*, 172−175.
(50) Wang, X.-B.; Woo, H.-K.; Kiran, B.; Wang, L.-S. Observation of Weak C-H···O Hydrogen-Bonding by Unactivated Alkanes. *Angew. Chem., Int. Ed.* **2005**, *44*, 4968−4972.
(51) Wang, X.-B.; Sergeeva, A. P.; Yang, J.; Xing, X.-P.; Boldyrev, A. I.; Wang, L. S. Photoelectron Spectroscopy of Cold Hydrated Sulfate Clusters, $SO_4^{2-}(H_2O)_n$ (n = 4−7): Temperature-Dependent Isomer Populations. *J. Phys. Chem. A* **2009**, *113*, 5567−5576.
(52) Kunz, W.; Lo Nostro, P.; Ninham, B. W. The Present State of Affairs with Hofmeister Effects. *Curr. Opin. Colloid Interface Sci.* **2004**, *9*, 1−18.
(53) Zhang, Y.; Cremer, P. S. Interactions between Macromolecules and Ions: The Hofmeister Series. *Curr. Opin. Chem. Biol.* **2006**, *10*, 658−663.
(54) Collins, K. D. Ions from the Hofmeister Series and Osmolytes: Effects on Proteins in Solution and in the Crystallization Process. *Methods* **2004**, *34*, 300−311.
(55) Vlachy, N.; Jagoda-Cwiklik, B.; Vácha, R.; Touraud, D.; Jungwirth, P.; Kunz, W. Hofmeister Series and Specific Interactions of Charged Headgroups with Aqueous Ions. *Adv. Colloid Interface Sci.* **2009**, *146*, 42−47.
(56) Baer, M. D.; Mundy, C. J. An Ab Initio Approach to Understanding the Specific Ion Effect. *Faraday Discuss.* **2013**, *160*, 89−101.
(57) Jungwirth, P.; Cremer, P. S. Beyond Hofmeister. *Nat. Chem.* **2014**, *6*, 261−263.
(58) Baer, M. D.; Pham, V.-T.; Fulton, J. L.; Schenter, G. K.; Balasubramanian, M.; Mundy, C. J. Is Iodate a Strongly Hydrated Cation? *J. Phys. Chem. Lett.* **2011**, *2*, 2650−2654.
(59) Wang, X.-B.; Yang, X.; Nicholas, J. B.; Wang, L.-S. Bulk-Like Features in the Photoemission Spectra of Hydrated Doubly Charged Anion Clusters. *Science* **2001**, *294*, 1322−1325.
(60) Zhou, J.; Santambrogio, G.; Brümmer, M.; Moore, D. T.; Wöste, L.; Meijer, G.; Neumark, D. M.; Asmis, K. R. Infrared Spectroscopy of Hydrated Sulfate Dianions. *J. Chem. Phys.* **2006**, *125*, 111102.
(61) O'Brien, J. T.; Prell, J. S.; Bush, M. F.; Williams, E. R. Sulfate Ion Patterns Water at Long Distance. *J. Am. Chem. Soc.* **2010**, *132*, 8248−8249.
(62) Dudev, T.; Lim, C. Factors Governing the Na^+ vs K^+ Selectivity in Sodium Ion Channels. *J. Am. Chem. Soc.* **2010**, *132*, 2321−2332.
(63) Dudev, T.; Lim, C. Determinants of K^+ vs Na^+ Selectivity in Potassium Channels. *J. Am. Chem. Soc.* **2009**, *131*, 8092−8101.
(64) Hay, B. P.; Bryantsev, V. S. Anion-Arene Adducts: C-H Hydrogen Bonding, Anion-π Interaction, and Carbon Bonding Motifs. *Chem. Commun.* **2008**, 2417−2428.
(65) Chifotides, H. T.; Dunbar, K. R. Anion−π Interactions in Supramolecular Architectures. *Acc. Chem. Res.* **2013**, *46*, 894−906.
(66) Wang, D.-X.; Wang, M.-X. Anion-π Interactions: Generality, Binding Strength, and Structure. *J. Am. Chem. Soc.* **2013**, *135*, 892−897.
(67) Kollman, P. A.; Allen, L. C. Theory of the Hydrogen Bond. *Chem. Rev.* **1972**, *72*, 283−303.
(68) Jeffrey, G.; Saenger, W. *Hydrogen Bonding in Biochemical Structures*; Springer-Verlag: Berlin, 1991.
(69) Meot-Ner, M. The Ionic Hydrogen Bond. *Chem. Rev.* **2005**, *105*, 213−284.
(70) Almeida, J.; Schobesberger, S.; Kürten, A.; Ortega, I. K.; Kupiainen-Määttä, O.; Praplan, A. P.; Adamove, A.; Amorim, A.; Bianchi, F.; Breitenlechner, M.; et al. Molecular Understanding of Sulphuric Acid-Amine Particle Nucleation in the Atmosphere. *Nature* **2013**, *502*, 359−363.
(71) Kulmala, M.; Kontkanen, J.; Junninen, H.; Lehtipalo, K.; Manninen, H. E.; Nieminen, T.; Petäjä, T.; Sipilä, M.; Schobesberger, S.; Rantala, P.; et al. Direct Observations of Atmospheric Aerosol Nucleation. *Science* **2013**, *339*, 943−946.
(72) Zhang, R.; Khalizov, A.; Wang, L.; Hu, M.; Xu, W. Nucleation and Growth of Nanoparticles in the Atmosphere. *Chem. Rev.* **2012**, *112*, 1957−2011.
(73) Wang, S. Y.; Zordan, C. A.; Johnston, M. V. Chemical Characterization of Individual, Airborne Sub-10-nm Particles and Molecules. *Anal. Chem.* **2006**, *78*, 1750−1754.
(74) Guo, S.; Hu, M.; Zamora, M. L.; Peng, J.; Shang, D.; Zheng, J.; Du, Z.; Wu, Z.; Shao, M.; Zeng, L.; et al. Elucidating Severe Urban Haze Formation in China. *Proc. Natl. Acad. Sci. U. S. A.* **2014**, *111*, 17373−17378.
(75) Zhang, R.; Wang, G.; Guo, S.; Zamora, M. L.; Ying, Q.; Lin, Y.; Wang, W.; Hu, M.; Wang, Y. Formation of Urban Fine Particulate Matter. *Chem. Rev.* **2015**, *115*, 3803−3855.
(76) McGraw, R.; Zhang, R. Multivariate Analysis of Homogeneous Nucleation Rate Measurements, Nucleation in the *p*-Toluic Acid/Sulfuric Acid/Water System. *J. Chem. Phys.* **2008**, *128*, 064508.
(77) Zhang, R. Getting to the Critical Nucleus of Aerosol Formation. *Science* **2010**, *328*, 1366−1367.
(78) Xu, W.; Zhang, R. Theoretical Investigation of Interaction of Dicarboxylic Acids with Common Aerosol Nucleation Precursors. *J. Phys. Chem. A* **2012**, *116*, 4539−4550.

DOI: 10.1021/acs.jpca.6b09784
J. Phys. Chem. A 2017, 121, 1389−1401

(79) Weber, K. H.; Morales, F. J.; Tao, F.-M. Theoretical Study on the Structure and Stabilities of Molecular Clusters of Oxalic Acid with Water. *J. Phys. Chem. A* **2012**, *116*, 11601−11617.
(80) Castleman, A. W. Experimental Studies of Ion Clustering-Relationship to Aerosol Formation Processes and Some Atmospheric Implications. *J. Aerosol Sci.* **1982**, *13*, 73−85.
(81) Zhao, J.; Khalizov, A.; Zhang, R. Y.; McGraw, R. Hydrogen-Bonding Interaction in Molecular Complexes and Clusters of Aerosol Nucleation Precursors. *J. Phys. Chem. A* **2009**, *113*, 680−689.
(82) Xu, Y.; Nadykto, A. B.; Yu, F.; Jiang, L.; Wang, W. Formation and Properties of Hydrogen-Bonded Complexes of Common Organic Oxalic Acid with Atmospheric Nucleation Precursors. *J. Mol. Struct.: THEOCHEM* **2010**, *951*, 28−33.
(83) Xu, Y.; Nadykto, A. B.; Yu, F.; Herb, J.; Wang, W. Interaction between Common Organic Acids and Trace Nucleation Species in the Earth's Atmosphere. *J. Phys. Chem. A* **2010**, *114*, 387−396.
(84) Nadykto, A. B.; Yu, F. Strong Hydrogen Bonding between Atmospheric Nucleation Precursors and Common Organics. *Chem. Phys. Lett.* **2007**, *435*, 14−18.
(85) Zhu, Y.-P.; Liu, Y.-R.; Huang, T.; Jiang, S.; Xu, K.-M.; Wen, H.; Zhang, W.-J.; Huang, W. Theoretical Study of the Hydration of Atmospheric Nucleation Precursors with Acetic Acid. *J. Phys. Chem. A* **2014**, *118*, 7959−7974.
(86) Zhang, R.; Suh, I.; Zhao, J.; Zhang, D.; Fortner, E. C.; Tie, X.; Molina, L. T.; Molina, M. J. Atmospheric New Particle Formation Enhanced by Organic Acids. *Science* **2004**, *304*, 1487−1490.
(87) Zhang, R.; Wang, L.; Khalizov, A. F.; Zhao, J.; Zheng, J.; McGraw, R. L.; Molina, L. T. Formation of Nanoparticles of Blue Haze Enhanced by Anthropogenic Pollution. *Proc. Natl. Acad. Sci. U. S. A.* **2009**, *106*, 17650−17654.
(88) Kawamura, K.; Ikushima, K. Seasonal Changes in the Distribution of Dicarboxylic Acids in the Urban Atmosphere. *Environ. Sci. Technol.* **1993**, *27*, 2227−2235.
(89) Limbeck, A.; Kraxner, Y.; Puxbaum, H. Gas to Particle Distribution of Low Molecular Weight Acids at Two Different Sites in Central Europe (Austria). *J. Aerosol Sci.* **2005**, *36*, 991−1005.
(90) Mochida, M.; Kitamori, Y.; Kawamura, K.; Nojiri, Y.; Suzuki, K. Fatty Acids in the Marine Atmosphere: Factors Governing Their Concentrations and Evaluation of Organic Films on Sea-salt Particles. *J. Geophys. Res.-Atmos.* **2002**, *107*, AAC 1-1−AAC 1-10.
(91) Zhang, D.; Zhang, R. Ozonolysis of α-Pinene and β-Pinene: Kientics and Mechanism. *J. Chem. Phys.* **2005**, *122*, 114308.
(92) Pathak, R. K.; Stanier, C. O.; Donahue, N. M.; Pandis, S. N. Ozonolysis of α-Pinene at Atmospherically Relevant Concentrations: Temperature Dependence of Aerosol Mass Fractions (yields). *J. Geophys. Res.* **2007**, *112*, D03201.
(93) Minofar, B.; Mucha, M.; Jungwirth, P.; Yang, X.; Fu, Y.-J.; Wang, X.-B.; Wang, L.-S. Bulk versus Interfacial Aqueous Solvation of Dicarboxylate Dianions. *J. Am. Chem. Soc.* **2004**, *126*, 11691−11698.
(94) Vonderach, M.; Ehrler, O. T.; Matheis, K.; Weis, P.; Kappes, M. M. Isomer-Selected Photoelectron Spectroscopy of Isolated DNA Oligonucleotides: Phosphate and Nucleobase Deprotonation at High Negative Charge States. *J. Am. Chem. Soc.* **2012**, *134*, 7830−7841.
(95) Jäger, P.; Brendle, K.; Schwarz, U.; Himmelsbach, M.; Armbruster, M. K.; Fink, K.; Weis, P.; Kappes, M. M. Q and Soret Band Photoexcitation of Isolated Palladium Porphyrin Tetraanions Leads to Delayed Emission of Nonthermal Electrons over Micro-second Time Scales. *J. Phys. Chem. Lett.* **2016**, *7*, 1167−1172.
(96) Bull, J. N.; West, C. W.; Verlet, J. R. R. On the Formation of Anions: Frequency-, Angle-, and Time-Resolved Photoelectron Imaging of the Menadione Radical Anion. *Chem. Sci.* **2015**, *6*, 1578−1589.
(97) Stavros, V. G.; Verlet, J. R. R. Gas-Phase Femtosecond Particle Spectroscopy: A Bottom-Up Approach to Nucleotide Dynamics. *Annu. Rev. Phys. Chem.* **2016**, *67*, 211−232.
(98) Chakrabarty, S.; Williams, E. R. The Effect of Halide and Iodate Anions on the Hydrogen-Bonding Network of Water in Aqueous Nanodrops. *Phys. Chem. Chem. Phys.* **2016**, *18*, 25483−25490.
(99) Rembert, K. B.; Paterová, J.; Heyda, J.; Hilty, C.; Jungwirth, P.; Cremer, P. S. Molecular Mechanisms of Ion-Specific Effects on Proteins. *J. Am. Chem. Soc.* **2012**, *134*, 10039−10046.
(100) Jungwirth, P. Ion Pairing: From Water Clusters to the Aqueous Bulk. *J. Phys. Chem. B* **2014**, *118*, 10333−10334.

DOI: 10.1021/acs.jpca.6b09784
J. Phys. Chem. A 2017, 121, 1389−1401